

# An Extended Boundary Integral Equation for Structures with Oscillatory Free-Surface Pressure

Chang-Ho Lee  
WAMIT, Inc.  
Chestnut Hill, Massachusetts, USA

J. Nicholas Newman  
Department of Mechanical Engineering, Massachusetts Institute of Technology  
Cambridge, Massachusetts, USA

**The conventional boundary integral equation for the solutions of linear wave-body interactions is extended to include the radiation solutions because of oscillatory pressures applied on the free surface. Coupled with the constraints that determine the pressure, the extended integral equation is applicable to various problems where a part of the bodies contains the free surface with oscillatory pressures. As illustrative examples, the analyses of wave interactions with an air-cushion vehicle and an oscillating water column device are made. As an additional application, we consider moon pool and gap resonances where the use of oscillatory pressures is an efficient way to introduce artificial damping to suppress excessive free-surface elevation of the potential flow.**

## INTRODUCTION

Structures such as oscillating water columns (OWCs) and air-cushion vehicles (ACVs) have air chambers with internal free surfaces (air/water interfaces). To analyze the behavior of these types of structures, the hydrodynamic and aerodynamic solutions in the respective regions are matched at the interface. In the context of the linearized potential theory, two alternative approaches are available. In one, the vertical displacement (or vertical velocity) of the free surface is represented by a set of prescribed modes, and the continuity of pressure is applied to determine the coefficients of these modes. In the second approach, the coefficients of the prescribed oscillatory pressure modes can be determined from the continuity of the vertical velocity. In the earlier applications of the panel methods, the former was preferred primarily because the relevant modes are defined by Neumann boundary conditions in the same manner as the conventional rigid body modes. The application of this approach to the analysis of OWCs is described in Lee et al. (1996) and of ACVs in Pinkster (1997), Pinkster et al. (1998), and Lee and Newman (2000).

The second approach, which was briefly described in Lee et al. (1996), is expanded in this paper. The characteristic acoustic wavelength is of  $O(1000\text{ m})$  at the frequency of  $O(1/s)$ . Since the air pressure varies slowly compared to the free-surface elevation, fewer modes are required in the second approach relative to the first, where a relatively large number of modes may be required to describe the vertical displacement of the interface. The advantages of the second approach include (i) little effort to find and describe an appropriate set of modes, (ii) direct interpretation of the computational results, and (iii) improved computational efficiency due to the reduced number of modes.

In the following section, the theory of the present approach is described. First, the pressure radiation potentials that satisfy the boundary condition of oscillatory pressure on the interface and homogeneous Neumann conditions on the body surface are defined. To be general, the air pressure is assumed to be spatially variable. Then the extended integral equation is derived to evaluate the pressure radiation potentials. Finally, a set of equations governing the motion of the body and the pressure on the interface is derived.

As a first computational example, a rectangular ACV model is analyzed, and the computational results obtained by two approaches are compared along with the experimental results from Pinkster et al. (1998). The OWC is analyzed next. The parameters, such as the optimum pressure and the capture width, are evaluated in a simpler manner, using the integrated forces corresponding to the pressure mode.

As a last example, we consider resonance of the free-surface elevation observed in the moon pool or in the gap between narrowly spaced vessels where the computations based on the linear potential flow often overpredict the wave height. Feng and Bai (2015), in their fully nonlinear simulations, found that the free-surface nonlinearity plays a minor role in suppressing the overpredicted resonance in the linear solutions. This confirms the experimental findings by Molin et al. (2009) that the viscous effects, primarily flow separation, account for the discrepancy between the linear solutions and measurements.

A few techniques have been proposed to introduce drag forces, simulating the viscous effects, to damp the resonant modes. For example, in Newman (2004), a flexible lid is placed on a part of the free surface, and the vertical displacement of the lid is subject to an appropriate damping force. Chen (2004) proposed a method that, in effect, applies a continuous pressure distribution on the free surface to extract energy out of the fluid. The effect of this pressure distribution can be taken into account efficiently by using a set of prescribed pressure modes. Using a couple of computational examples, we show that the use of pressure modes is a simple and effective alternative to the flexible lid to damp the resonant behavior.

---

Received August 1, 2015; updated and further revised manuscript received by the editors October 30, 2015. The original version (prior to the final updated and revised manuscript) was presented at the Twenty-fifth International Ocean and Polar Engineering Conference (ISOPE-2015), Kona, Hawaii, June 21–26, 2015.

**KEY WORDS:** Wave-body interaction, boundary integral equation, air-cushion vehicle, oscillatory water column, gap resonance.

## FORMULATION

Cartesian coordinates  $\mathbf{x} = (x, y, z)$  are used with the vertical  $z$ -axis positive upward and with  $z = 0$  the plane of the undisturbed free surface. We consider a rigid body floating on the free surface partially supported by the pressure in the air chamber or a fixed body with an air chamber as in an OWC. The wetted body surface is denoted by  $S_b$ , the fixed surface of the air chamber by  $S_c$ , and the horizontal air and water interface by  $S_i$ . The complete closed surface bounding the air chamber is denoted by  $S_a = S_c + S_i$ . The complete boundary surface of the water on and inside the body is  $S_w = S_b + S_i$ . The free surface outside the body is denoted by  $S_f$ .

The fluid velocity is represented by the gradient of the velocity potential  $\Phi$ , which satisfies the Laplace equation:

$$\nabla^2 \Phi = 0 \quad (1)$$

in the fluid domain. Assuming regular incident waves, the velocity potential can be expressed in the complex form:

$$\Phi = \Re \{ \phi e^{i\omega t} \} \quad (2)$$

where  $\Re$  denotes the real part,  $\omega$  is the frequency of the incident wave, and  $t$  is time.

From the linearized Bernoulli equation, the dynamic pressure on the free surface is:

$$p(x, y, z) = -i\rho\omega\phi(x, y, z) - \rho g\zeta \quad (3)$$

where  $\rho$  is the water density,  $g$  is gravity, and  $\zeta$  is the wave elevation relative to the mean position of the free surface. Combined with the kinematic condition  $\phi_z = i\omega\zeta$ , it follows that:

$$\phi_z - K\phi = -\frac{i\omega}{\rho g} p \quad \text{on } S_i \text{ and } S_f \quad (4)$$

where  $K = \omega^2/g$ . Here the subscript  $z$  denotes the partial derivative with respect to  $z$ .

In Eq. 4, it is convenient to express the oscillatory pressure distribution, yet to be determined, in terms of prescribed modes in a form:

$$p_o(x, y) \equiv p(x, y, z_l) = -\rho g \sum_{j=7}^{6+N_p} \xi_j n_j(x, y) \quad (5)$$

where  $z_l \leq 0$  is the mean vertical coordinate of  $S_i$ ,  $n_j(x, y)$  is the nondimensional pressure distribution mode,  $\xi_j$  is the model amplitude coefficient with the dimension of length, and  $N_p$  is the number of modes. When  $p_o$  is assumed to be uniform,  $N_p = 1$  and  $n_7(x, y) = 1$ . On  $S_f$ ,  $p(x, y, 0) = 0$ .

On  $S_b$ ,  $\phi$  is subject to the Neumann boundary condition:

$$\phi_n = \mathbf{V} \cdot \mathbf{n} \quad (6)$$

where  $\mathbf{V}(\mathbf{x})$  is the velocity vector of the points on the body surface and  $\mathbf{n}$  denotes the normal vector.

The velocity potential can be expressed in terms of the diffraction and radiation components:

$$\phi = \phi_D + \phi_R \quad (7)$$

where

$$\phi_D = \phi_I + \phi_S \quad (8)$$

$$\phi_R = i\omega \sum_{j=1}^{6+N_p} \xi_j \phi_j \quad (9)$$

In Eq. 9, the coefficients  $\xi_j$  for  $1 \leq j \leq 6$  are the displacements in surge, sway, heave, roll, pitch, and yaw modes. The incident wave system is defined by the potential:

$$\phi_I = \frac{igA \cosh[k(z+h)]}{\omega \cosh kh} \exp(-ik(x \cos \beta + y \sin \beta)) \quad (10)$$

where  $A$  is the amplitude,  $k$  is the finite-depth wave number,  $h$  is the fluid depth, and  $\beta$  is the wave angle relative to the positive  $x$ -axis.

We define  $n_j$  such that  $(n_1, n_2, n_3) = \mathbf{n}$ ,  $(n_4, n_5, n_6) = \mathbf{x} \times \mathbf{n}$ , and  $n_j = 0$  for  $j \geq 7$  on  $S_b$ . On  $S_i$ ,  $n_j = 0$  for  $1 \leq j \leq 6$  and, for  $j \geq 7$ ,  $n_j$  is the same as the nondimensional pressure distribution mode in Eq. 5. With this definition, each component in Eq. 9 is subject to the conditions:

$$\phi_{j_n} = n_j \quad \text{on } S_b \quad (11)$$

$$\phi_{j_z} - K\phi_j = n_j \quad \text{on } S_i \quad (12)$$

and the diffraction potential is subject to the conditions:

$$\phi_{D_n} = 0 \quad \text{on } S_b \quad (13)$$

$$\phi_{D_z} - K\phi_D = 0 \quad \text{on } S_i \quad (14)$$

The velocity potentials in Eqs. 7 to 9 are also subject to the homogeneous free-surface condition on  $S_f$  and, with the exception of  $\phi_I$ , to the radiation condition of outgoing waves in the far field.

$\phi_j$  and  $\phi_D$  can be derived from appropriate variants of Green's theorem, using the free-surface Green function  $G(\xi; \mathbf{x})$ , which satisfies the homogeneous form of the free-surface boundary condition on  $S_f$ . The resulting integral equations can be summarized as:

$$\begin{aligned} & \left( \frac{2}{4} \right) \pi \phi_j(\mathbf{x}) + \iint_{S_w} \phi_j(\xi) \mathcal{L}(G(\xi; \mathbf{x})) d\xi \\ & = \iint_{S_w} n_j(\xi) G(\xi; \mathbf{x}) d\xi \end{aligned} \quad (15)$$

and

$$\left( \frac{2}{4} \right) \pi \phi_D(\mathbf{x}) + \iint_{S_w} \phi_D(\xi) \mathcal{L}(G(\xi; \mathbf{x})) d\xi = 4\pi \phi_I(\mathbf{x}) \quad (16)$$

where

$$\mathcal{L} = \begin{cases} \partial/\partial n_\xi & \xi \in S_b \\ \partial/\partial n_\xi - K & \xi \in S_i \end{cases} \quad (17)$$

The factor  $2\pi$  is applied if the boundary surface is below  $z = 0$ , and the factor  $4\pi$  is applied if the boundary surface is on  $z = 0$ . In the latter case, the integral over  $S_i$  on the left-hand sides of Eqs. 15 and 16 vanishes, since the Green function satisfies the homogeneous free-surface condition.

$\xi_j$  in Eq. 9 is derived in part from the equations of motion corresponding to the rigid body modes  $1 \leq j \leq 6$ . The total forces and moments include the hydrodynamic and hydrostatic pressure on  $S_b$  and the aerodynamic pressure on  $S_c$ . (Hydrostatic pressure  $-\rho g z_l$  on  $S_c$  affects the restoring moments of the roll and pitch modes and should be included.) The aerostatic pressure can be neglected on the assumption  $c_o \gg g/w$  where  $c_o$  is the sound

velocity. Additional equations for  $7 \leq j$  are obtained by invoking continuity of the vertical velocity across  $S_i$  in the form:

$$\frac{-i\rho g}{\omega} \left( \iint_{S_i} V_z(x, y) n_i dS - \iint_{S_i} \phi_z n_i dS \right) = 0 \quad (18)$$

where  $V_z(x, y)$  is the vertical velocity distribution of air on  $S_i$ . Upon substituting the velocity potentials Eqs. 8 and 9, subject to the boundary conditions Eqs. 11 to 14, the second term of Eq. 18 can be expressed in terms of the hydrodynamic and hydrostatic forces as described below. The force represented by the first term is dependent on the aerodynamic solution in the air chamber.

The complete set of equations for  $\xi_j$  can be summarized as:

$$\sum_{j=1}^{6+N_p} [-\omega^2(M_{ij} + A_{ij} + A_{ij}^a) + i\omega(B_{ij} + B_{ij}^a) + (C_{ij} + C_{ij}^a)] \xi_j = X_i. \quad (19)$$

Here  $M_{ij}$  is the inertia of the structure, and  $M_{ij} = 0$  for  $7 \leq i$  or  $7 \leq j$ . The radiation pressure forces are represented by the coefficients:

$$A_{ij} - \frac{i}{\omega} B_{ij} = \rho \iint_{S_w} \phi_j n_i dS \quad (20)$$

The coefficients are symmetric, which can be easily verified by applying Green's theorem to  $\phi_i$  and  $\phi_j$  subject to the boundary conditions Eqs. 11 and 12. The exciting force components are:

$$X_i = -i\omega\rho \iint_{S_w} \phi_D n_i dS \quad (21)$$

The hydrostatic coefficients  $C_{ij}$  are the same as the conventional rigid body motions for  $i \leq 6$  and  $j \leq 6$ , with the understanding that integration of the hydrostatic pressure is extended over  $S_b$  and the buoyancy force includes the hydrostatic pressure  $-\rho g z_i$  exerted on  $S_c$ , as shown in WAMIT (2015). For  $7 \leq i$  and  $7 \leq j$ :

$$C_{ij} = -\rho g \iint_{S_i} n_i n_j dS \quad (22)$$

When  $p_o$  is uniform,  $C_{77} = -\rho g S_i$ , where  $S_i$  is understood as the area of the interface.

The superscript  $a$  in the coefficients  $A_{ij}^a$ ,  $B_{ij}^a$ , and  $C_{ij}^a$  denotes that they depend on the solution of the linearized aerodynamic problem in the air chamber subject to the oscillatory pressure  $p_o$  on  $S_i$ , appropriate boundary conditions on  $S_c$ , and other effects in the chamber. They may be considered as the external constraints on  $\xi_j$  in the equations of motion Eq. 19 and are evaluated from the following relation:

$$\sum_{j=1}^{6+N_p} (-\omega^2 A_{ij}^a + i\omega B_{ij}^a + C_{ij}^a) \xi_j = \begin{cases} -\iint_{S_c} P(\mathbf{x}) N_i dS & \text{for } 1 \leq i \leq 6 \\ \frac{-i\rho g}{\omega} \iint_{S_i} V_z(x, y) n_i dS & \text{for } 7 \leq i \end{cases} \quad (23)$$

where  $P(\mathbf{x})$  is the aerodynamic pressure,  $(N_1, N_2, N_3) = \mathbf{n}$ , and  $(N_4, N_5, N_6) = \mathbf{x} \times \mathbf{n}$  on  $S_c$ .

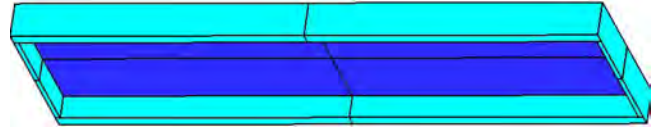


Fig. 1 Perspective view of the submerged portion of the model,  $S_w = S_b + S_i$ , viewed from below. Part of the air/water interface,  $S_i$ , is visible inside the vertical walls.

## AIR-CUSHION VEHICLE (ACV)

We consider the model with one air chamber (shown in Fig. 1) used by Pinkster et al. (1998) for their free-floating model tests. The dimensions of the submerged portion of the model are length 2.5 m, beam 0.78 m, and draft 0.15 m. The wall thickness is 0.02 m at the ends and 0.06 m at the sides. The air chamber extends from  $-0.05$  m below the exterior free surface to 0.13 m above. The water depth is 2.5 m, the center of gravity is at  $(0, 0, 0.15)$  m, and the pitch radius of gyration about this point is 0.751 m. The relevant acoustic added mass and the restoring force coefficients used in the computations are derived from the solution of the Helmholtz equation in the Appendix.

Figure 2 shows the heave and pitch responses computed at 100 frequencies. The higher-order panel method is used with panels of approximately 0.8 m length. The computational results are converged, with respect to the panel length, up to the graphical

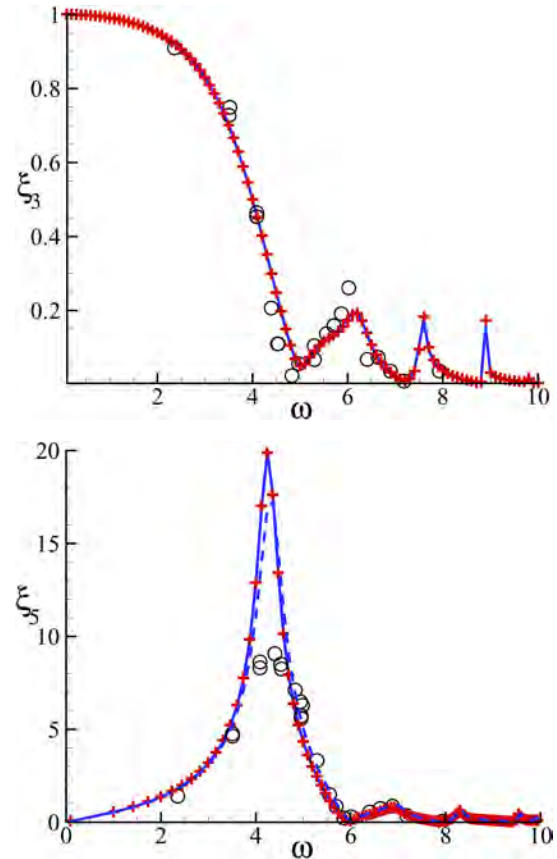


Fig. 2 Heave and pitch response amplitude operators (RAOs) normalized by the incident wave amplitudes  $A$  and  $A/L$ , respectively.  $L = 2.5$  m is the length of the model. The lines are computed by the present method, the pluses (+) by Lee and Newman (2000), and the circles (o) by Pinkster et al. (1998). The dashed line corresponds to the results with a uniform pressure only.

accuracy. The results computed by the current approach using two pressure modes, the uniform and the first antisymmetric modes in  $x$  in Eq. 38, are compared with the corresponding results in Lee and Newman (2000) computed by the first approach using 32 Fourier modes. The response amplitude operators (RAOs) computed by these two approaches are identical, including the resonant peaks. The pitch RAO without the antisymmetric pressure mode is also presented. The latter shows some difference near the resonant peak where the pitch RAO is approximately 10 times the wave slope because of a strong sloshing resonance. The computational results agree quite well with the experimental results, except in the vicinity of the resonant peak of the pitch mode. The difference may be attributed to viscous and nonlinear effects.

### OSCILLATING WATER COLUMN (OWC) DEVICE

We consider one of the oscillating water column (OWC) devices considered in Lee et al. (1996). The configuration of this device is illustrated in Fig. 3. Because the device is sufficiently small, a uniform pressure distribution is assumed in the following.

As shown in Evans (1982), the power transferred across the interior free surface is equal to the time-average of the rate of energy flux, which takes a form:

$$\begin{aligned} \frac{dE}{dt} &= \iint_{S_i} \overline{P\Phi_z} dS = \frac{1}{2} \Re \left\{ p_o^* \iint_{S_i} \phi_z dS \right\} = \frac{\omega^2}{2g} \Re \left\{ p_o^* \iint_{S_i} \phi dS \right\} \\ &= \frac{\omega \Re(ip_o^* X_7)}{2\rho g} - \frac{\omega^2 |p_o|^2 B_{77}}{2\rho^2 g^2} \end{aligned} \quad (24)$$

The optimum pressure is the zero of the derivative of Eq. 24 with respect to  $p_o$  and is given by:

$$P_o = \frac{i\rho g X_7}{2\omega B_{77}} \quad (25)$$

It is customary to normalize the energy flux rate in respect to the corresponding rate of input in the incident wave system per unit width of the wave crests, equal to  $(1/2)\rho g A^2 v_g$  where  $v_g = d\omega/dk$  is the group velocity. This ratio is known as the capture width. The capture width, corresponding to the optimum pressure  $P_o$ , is denoted by  $W_o$ , which represents the theoretically maximum transfer rate.

The optimum pressure and capture width are compared with corresponding parameters of a practical model in the following.

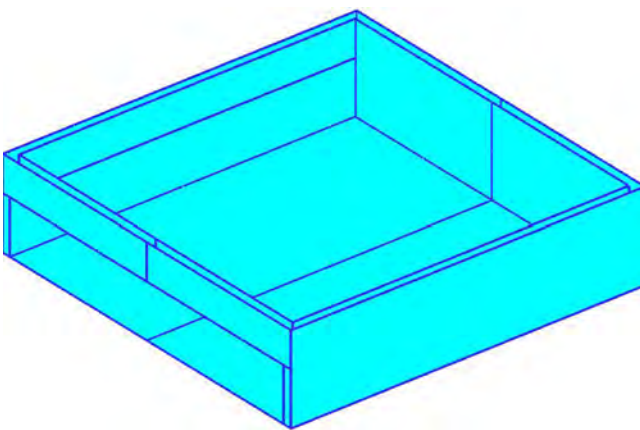


Fig. 3 Configuration of the submerged portion of the OWC. The horizontal dimensions are 20 m x 20 m, the draft is 5 m, and the wall thickness is 0.5 m. The height of the aperture on the OWC is 3 m. The OWC is mounted on the sea bottom.

In the context of linear analysis, the behavior of the turbine is modeled by a linearized damping force that is proportional to the average rate of air flow across the interface such that:

$$B_i \iint_{S_i} V_z dS = p_o S_i^2 \quad (26)$$

Here  $B_i$  is the damping coefficient, and  $S_i$  on the right-hand side is understood as the surface area of the interface. Upon substituting the relations Eq. 26 and  $p_o = -\rho g \xi_7$  into Eq. 23, we find that the damping coefficient for the uniform pressure mode,  $\xi_7$ , is:

$$B_{77}^a = \frac{(\rho g)^2 S_i^2}{\omega^2 B_i} = \frac{C_{77}^2}{\omega^2 B_i} \quad (27)$$

$\xi_7$  is then evaluated in Eq. 19 with the result:

$$p_o = \frac{-\rho g X_7}{(C_{77} - \omega^2 A_{77}) + i\omega(B_{77} + B_{77}^a)} \quad (28)$$

The rate of the energy flux can be expressed in the form:

$$\frac{dE}{dt} = \frac{1}{2} \Re \left\{ p_o^* \iint_{S_i} V_z dS \right\} = \frac{S_i^2}{2B_i} |p_o|^2 = \frac{\omega^2 S_i^2}{2C_{77}^2} B_{77}^a |p_o|^2 \quad (29)$$

In Eq. 29, the maximum rate occurs when:

$$B_{77}^a(\omega) = \sqrt{B_{77}^2 + (C_{77} - \omega^2 A_{77})^2 / \omega^2} \quad (30)$$

The pressure and the capture width corresponding to the maximum rate are denoted by  $P_t$  and  $W_t$ .  $P_t = P_o$  and  $W_t = W_o$  at the resonance frequency of the pumping mode,  $\omega = \sqrt{C_{77}/A_{77}}(\omega)$ , where Eq. 29 is reduced to Eq. 24.

The computational results are shown in Fig. 4. In the computations, the wavelength of the incident wave varies approximately from 30 m to 1,200 m. The corresponding nondimensional wave number,  $kL$ , varies from 0.05 to 2 where  $L$  is taken as 10 m, the half-beam of the OWC. We consider the case of head seas, where the direction of the incident wave is toward the aperture face at a right angle.  $X_7$  and  $B_{77}$  show that the resonance of the pumping mode occurs near  $kL = 0.5$  and that of the sloshing mode near  $kL = 1.7$ .  $P_t$  and  $W_t$  are close to  $P_o$  and  $W_o$  between  $kL = 0.3$  and  $kL = 0.5$ , over which the ratio  $|(C_{77} - \omega^2 A_{77})/\omega B_{77}|$  is small and flat, as shown in Fig. 5.

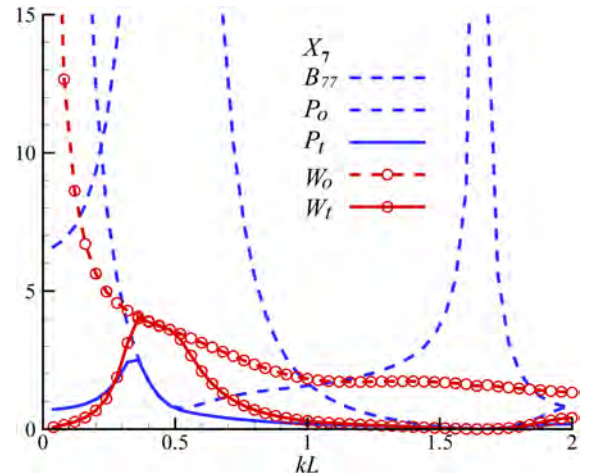


Fig. 4 The figure shows  $X_7$ ,  $B_{77}$ ,  $P_o$ , and  $W_o$ , normalized by  $\rho g A^2$ ,  $\rho L^3 \omega$ ,  $\rho g A$ , and  $L$ , respectively, against  $kL$ . It also shows normalized  $P_t$  and  $W_t$ .

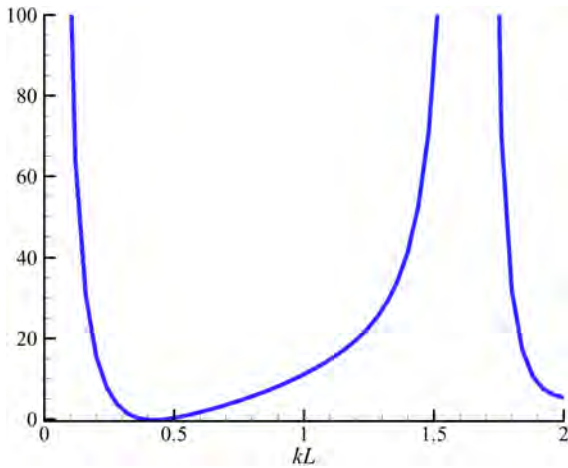


Fig. 5 The figure shows the ratio  $|(C_{77} - \omega^2 A_{77})/\omega B_{77}|$

MOON POOL/GAP RESONANCE

We illustrate the use of the pressure mode to damp the resonant modes in this section. For this purpose, it is convenient to introduce an additional body or bodies that consist of one or more interfaces  $S_i$  on the free surface of a moon pool or a gap.  $S_i$ , in this context, will be referred to as the “pressure patch.” The multibody interaction among the physical bodies and the bodies represented by the pressure patches can be analyzed by the method described in the second section. The external damping coefficients  $B_i$  or  $B_{ij}^a$  are now artificial parameters that may be adjusted in accordance with the experimental results.

We first consider a vertical circular cylinder with a concentric circular moon pool in infinite water depth. The draft and radius of the cylinder are 1 m and 0.5 m, respectively. The radius of the moon pool is 0.25 m. The resonant pumping mode in the moon pool occurs at approximately  $Kd = 0.8$  where  $d$  denotes the draft. The computational results using a circular pressure patch are compared with the corresponding results using a circular lid, which, like the pressure patch, is treated as a separate body. The cylinder and the lid are allowed to move in the heave mode only. Assuming a constant pressure, the pressure patch absorbs the energy at the rate shown in Eq. 29.

To compare the two methods, equivalent values of  $B_i$  and  $B_{77}^a$  are obtained by converting one constant coefficient to another using the relation Eq. 27. However, the converted coefficient is an inverse quadratic in  $\omega$ , which is cumbersome to use. To simplify the conversion, one converted value corresponding to  $\omega = 0.78$ , which is close to the resonance frequency, is used for all frequencies. It is smaller than the exact value when  $\omega < 0.78$  and vice versa. (A smaller  $B_{77}^a$  means larger impedance in the vertical motion of the free surface.) Simplified conversion is reasonable when the effects of the external damping force are expected to be small except in the vicinity of the resonance frequencies.

The free-surface elevation in the moon pool is shown in Fig. 6. The computational results using a lid are very close to the corresponding results using a pressure patch except for small differences due to the simplified conversion.

In the next example, we consider two identical rectangular barges fixed in infinite water depth. The length, beam, and draft of the barge are 160 m, 30 m, and 15 m, respectively. Two barges are separated by 8 m, as shown in Fig. 7. Two resonant free-surface modes are considered. One mode is symmetric in  $x$  about the midpoint of the gap and the other is antisymmetric. The moduli of

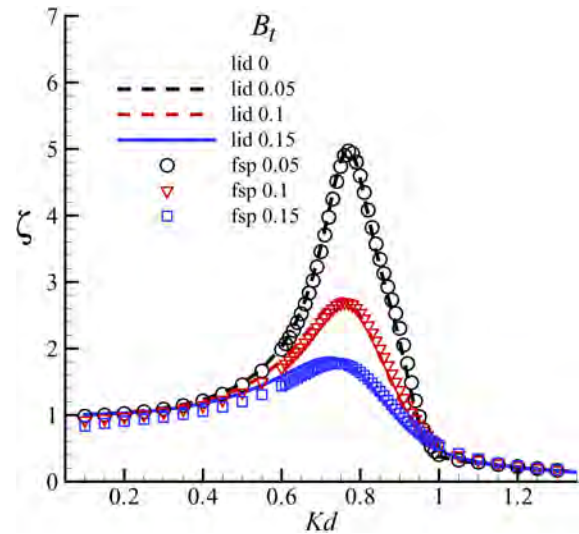


Fig. 6 Modulus of the free-surface elevation computed with three different values of damping coefficients as well as without external damping force. The coefficients for the heave mode of the lid are  $B_i = 0.05\rho, 0.1\rho,$  and  $0.15\rho$  in kg/s. The coefficients for the heave mode of the cylinder are  $2B_i$ . “lid” denotes the results obtained using a lid, and “fsp” denotes those using a pressure patch. For the latter,  $B_{77}^a$  is obtained by Eq. 27 with  $\omega = 0.78$ .

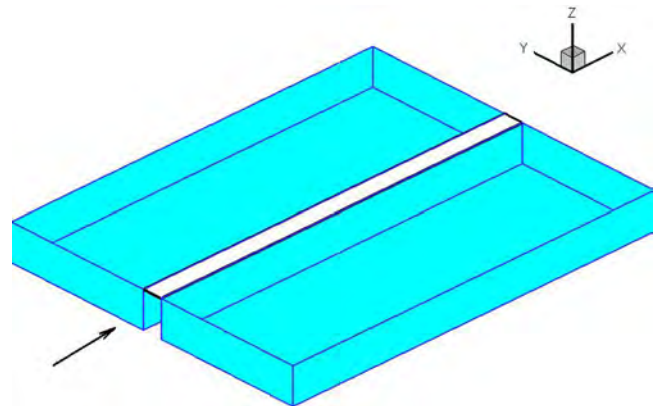


Fig. 7 Twin barges with a pressure patch on the free surface between the barges

the free-surface elevation of the two resonant modes are shown in Fig. 8 by the lines corresponding to  $B_{77}^a = B_{88}^a = \infty$ .  $B_{77}^a$  and  $B_{88}^a$  are damping coefficients for two pressure modes that are described below.

Inferred from the resonant modes, a symmetric pressure mode of the form,  $n_7(x) = \cos(3\pi x/L)$ , and an antisymmetric pressure mode,  $n_8(x) = \sin(2\pi x/L)$ , are considered in the computation. Here  $L$  denotes the length of the barge. ( $j = 7$  represents the uniform pressure mode in this paper except in this example. Here it denotes the nonuniform symmetric mode.) The ratio of the damping coefficients of the two pressure modes is determined such that the amplitudes of the two resonant modes are reduced at a similar rate. Figure 8 shows the moduli of the free-surface elevations computed with four different values of  $B_{77}^a$  and  $B_{88}^a$ .

Other pressure modes that are not orthogonal to the resonant modes may well be used. In this case, however, the damping coefficients should be adjusted separately. Another practical method, which may be useful for more complex geometry of the gap, is to

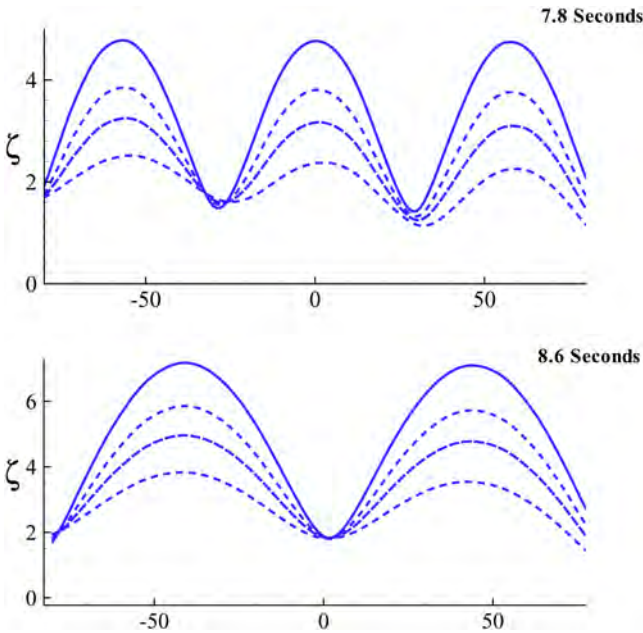


Fig. 8 Modulus of the free-surface elevation along the  $x$ -axis on the gap. Four results are shown corresponding to four different sets of damping coefficients.  $B_{77}^a = \infty, 1.E9, 5.E8,$  and  $2.5E8$  in  $\text{kg/s}$ , and  $B_{88}^a$  is 1.4 times  $B_{77}^a$ . The elevation decreases as  $B_{ii}^a$  decreases.  $B_{ii}^a = \infty$  corresponds to the free-surface elevation with two barges only, without considering the pressure modes.

divide the gap using multiple uniform pressure patches. In general, the damping coefficient for each uniform pressure mode should be determined separately. For the current example, three or six pressure patches of equal length may be used for the symmetric mode, and two or four patches may be used for the antisymmetric mode. The same damping coefficient may be assumed on all patches in these cases because of symmetry.

The free-surface elevation is given by:

$$\zeta(x, y) = -\frac{i\omega}{g}\phi(x, y) + \sum_{j=7}^{6+N_p} \xi_j n_j(x, y) \quad (31)$$

where  $\xi_j$ s are the amplitudes of the pressure modes on the patch to which  $(x, y)$  belongs. It is straightforward to obtain the elevation on the patches with a uniform pressure where  $n_j = 1$ .

## CONCLUSIONS

We have extended the conventional integral equation to obtain the radiation solutions because of oscillatory pressure on the free surface directly. The computational results are validated by making comparison with the existing indirect approach.

Though both approaches are applicable to the analysis of the structures with internal air/water interfaces, the direct approach has a few advantages as illustrated in the computational examples. As shown in the analysis of the ACV, the number of required modes is significantly smaller in the current approach. This is particularly so when the area of the interface, compared to the incident wavelength, becomes larger. As illustrated in the analysis of an oscillating water column (OWC) that is relative small, the resonant behavior can be described more accurately using the current approach. Also, it is straightforward to obtain the parameters, such as the optimum pressure and the capture width, from the hydrodynamic parameters of the pressure mode. We have also shown that artificial damping

can be introduced on the free surface of a gap in a simpler manner using oscillatory pressure.

The hydrodynamic analyses are performed using the panel program WAMIT. The higher-order method is used in all computations, as it is expected that the low-order method is not as efficient nor as accurate in the vicinity of resonances that are considered in all examples.

## REFERENCES

- Chen, XB (2004). "Hydrodynamics in Offshore and Naval Applications Part I," *6th Int Conf Hydrodyn*, Keynote Lecture, Perth, Australia.
- Evans, DV (1982). "Wave Power Absorption by Systems of Oscillating Surface Pressure Distributions," *J Fluid Mech*, 114, 481-499. <http://dx.doi.org/10.1017/S0022112082000263>.
- Feng, X, and Bai, W (2015). "Wave Resonances in a Narrow Gap Between Two Barges Using Fully Nonlinear Numerical Simulation," *J Appl Ocean Res*, 50, 119-129. <http://dx.doi.org/10.1016/j.apor.2015.01.003>.
- Lee, C-H, and Newman, JN (2000). "Wave Effects on Large Floating Structures with Air Cushions," *J Mar Struct*, 13(4), 315-330. [http://dx.doi.org/10.1016/S0951-8339\(00\)00014-9](http://dx.doi.org/10.1016/S0951-8339(00)00014-9).
- Lee, C-H, Newman, JN, and Nielsen, FG (1996). "Wave Interaction with an Oscillating Water Column," *Proc 6th Int Offshore Polar Eng Conf*, Los Angeles, CA, USA, ISOPE, 1, 82-90.
- Molin, B, Remy, F, Camhi, A, and Ledoux, A (2009). "Experimental and Numerical Study of the Gap Resonances in-between Two Rectangular Barges," Presented at *13th Congr Int Marit Assoc Mediterr*, Istanbul, Turkey.
- Newman, JN (2004). "Progress in Wave Load Computations on Offshore Structures," *23rd Int Conf Ocean Offshore Arct Eng*, Invited Lecture, Vancouver, Canada.
- Pinkster, JA (1997). "The Effect of Air Cushions Under Floating Offshore Structures," *Proc 8th Int Conf Behav Offshore Struct*, Delft, Netherlands, BOSS, 2, 143-158.
- Pinkster, JA, Fauzi, A, Inoue, Y, and Tabeta, S (1998). "The Behavior of Large Air Cushion Supported Structures in Waves," *Proc 2nd Int Conf Hydroelast Mar Technol*, Fukuoka, Japan, 497-505.
- WAMIT (2015). *WAMIT V7 User Manual*, WAMIT, Inc, Chestnut Hill, MA, USA, <http://www.wamit.com/manual.htm>.

## APPENDIX

We consider a rectangular air chamber of length  $2a$  and width  $2b$  and extending between  $z_l \leq z \leq z_h$ . The height of the chamber is denoted by  $2c = z_h - z_l$ .  $x = y = 0$  coincides with the center of the air chamber.

The motion of air is represented by the velocity potential:

$$\Re \{ \Phi(\mathbf{x}) e^{i\omega t} \}$$

where  $\Phi(\mathbf{x})$  is governed by the Helmholtz equation:

$$\nabla^2 \Phi + K_a^2 \Phi = 0 \quad (32)$$

Here  $K_a = \omega/c_0$  is the acoustic wave number, and  $c_0$  is the sound velocity.

The air pressure on  $S_i$  is:

$$P(x, y, z_l) = -i\rho_a \omega \Phi(x, y, z_l) \quad (33)$$

and it is the same as  $p_o$  in Eq. 5. On  $S_c$ , the velocity potential is subject to the Neumann boundary condition:

$$\Phi_n = \mathbf{V} \cdot \mathbf{n} \quad (34)$$

where  $\mathbf{V}(\mathbf{x})$  is the velocity vector of a point on  $S_c$  and  $\mathbf{n}$  denotes the normal vector.

In accordance with Eq. 9, the potential is expanded in a form:

$$\Phi = i\omega \sum_{j=1}^{6+N_p} \xi_j \Phi_j \quad (35)$$

For  $j \leq 6$ , the components in Eq. 35 are subject to the conditions:

$$\Phi_{j_n} = N_j \text{ on } S_c \quad \text{and} \quad \Phi_j = 0 \text{ on } S_i \quad (36)$$

and  $7 \leq j$

$$\Phi_{j_n} = 0 \text{ on } S_c \quad \text{and} \quad \Phi_j = -\frac{\rho}{\rho_a} \frac{1}{K} n_j(x, y) \text{ on } S_i \quad (37)$$

where  $N_j$  is provided in Eq. 23. The pressure is represented by a complete set of orthogonal Fourier modes such that:

$$n_j(x, y) = \begin{pmatrix} \cos u_m x \\ \sin u_m x \end{pmatrix} \begin{pmatrix} \cos v_l y \\ \sin v_l y \end{pmatrix} \quad (38)$$

where

$$u_m = \frac{m\pi}{2a} \quad \text{and} \quad v_l = \frac{l\pi}{2b} \quad (39)$$

and the integers  $m$  and  $l$  are 0 and even for the modes corresponding to the cosine or odd for sine.

For brevity, we assume that the incident wave travels along the  $x$ -axis and consider the components that are independent of  $y$ . The potentials corresponding to three rigid body modes are derived in the form:

$$\begin{aligned} \Phi_1 &= \frac{4}{\pi} \sum_{n=1}^{\infty} \frac{1}{n} \frac{\sin \delta_n x \sin \gamma_n z'}{\delta_n \cos \delta_n a} \\ \Phi_3 &= \frac{\sin K_a z'}{K_a \cos 2K_a c} \\ \Phi_5 &= z_l \Phi_1 + \frac{16c}{\pi^2} \sum_{n=1}^{\infty} \frac{s_n}{n^2} \frac{\sin \delta_n x \sin \gamma_n z'}{\delta_n \cos \delta_n a} \\ &\quad - \frac{8a}{\pi^2} \sum_{n=1}^{\infty} \frac{s_n}{n^2} \frac{\sin \alpha_n x \sin \beta_n z'}{\beta_n \cos 2\beta_n c} \end{aligned} \quad (40)$$

where  $n$  is odd and  $\alpha_n = n\pi/(2a)$ ,  $\gamma_n = n\pi/(4c)$ ,  $\beta_n = \sqrt{K_a^2 - \alpha_n^2}$ ,  $\delta_n = \sqrt{K_a^2 - \gamma_n^2}$ ,  $s_n = \sin(n\pi/2)$ , and  $z' = z - z_l$ . For  $7 \leq j$ , the appropriate potentials satisfying Eq. 37 are:

$$\Phi_j(\mathbf{x}) = -\frac{\rho}{\rho_a} \frac{1}{K} n_j(x, y) \frac{\cos w_j(2c - z')}{\cos 2w_j c} \quad (41)$$

where  $w_j = \sqrt{K_a^2 - (u_m^2 + v_l^2)}$ .

The aerodynamic added mass and restoring force coefficients in Eq. 23 take the forms:

$$\begin{aligned} A_{11}^a &= \rho_a \frac{16b}{\pi} \sum_{n=1}^{\infty} \frac{1}{n} \frac{1}{\gamma_n} \frac{\tan \delta_n a}{\delta_n} \\ A_{33}^a &= \rho_a 4ab \frac{\tan 2K_a c}{K_a} \\ A_{51}^a &= \rho_a \frac{16b}{\pi} \left[ a \sum_{n=1}^{\infty} \frac{s_n}{n} \frac{1}{\delta_n^2} + z_l \sum_{n=1}^{\infty} \frac{1}{n} \frac{1}{\gamma_n} \frac{\tan \delta_n a}{\delta_n} \right. \\ &\quad \left. \sum_{n=1}^{\infty} \frac{s_n}{n} \left( \frac{1}{\gamma_n^2} - \frac{1}{\delta_n^2} \right) \frac{\tan \delta_n a}{\delta_n} \right] \\ A_{55}^a &= \rho_a \left\{ z_l A_{51}^a + \frac{64bc}{\pi^2} \left[ a \sum_{n=1}^{\infty} \frac{1}{n^2} \frac{1}{\delta_n^2} \right. \right. \\ &\quad \left. \left. + z_l \sum_{n=1}^{\infty} \frac{s_n}{n^2} \frac{1}{\gamma_n} \frac{\tan \delta_n a}{\delta_n} \sum_{n=1}^{\infty} \frac{1}{n^2} \left( \frac{1}{\gamma_n^2} - \frac{1}{\delta_n^2} \right) \frac{\tan \delta_n a}{\delta_n} \right] \right. \\ &\quad \left. + \frac{32ab}{\pi^2} \left[ \sum_{n=1}^{\infty} \frac{1}{n^2} \left( \frac{1}{\alpha_n^2} - \frac{1}{\beta_n^2} \right) \frac{\tan 2\beta_n c}{\beta_n} \right. \right. \\ &\quad \left. \left. + (z_l + 2c) \sum_{n=1}^{\infty} \frac{1}{n^2} \frac{1}{\beta_n^2} - z_l \sum_{n=1}^{\infty} \frac{1}{n^2} \frac{1}{\beta_n^2 \cos 2\beta_n c} \right] \right\} \quad (42) \end{aligned}$$

and

$$\begin{aligned} C_{1j}^a &= 4\rho g b s_m \frac{\tan 2w_j c}{w_j} \\ C_{37}^a &= \rho g S_i \frac{1}{\cos 2K_a c} \\ C_{5j}^a &= 4\rho g b s_m \left[ z_l \frac{\tan 2w_j c}{w_j} + \frac{1}{\cos 2w_j c} \left( \frac{1}{w_j^2} - \frac{1}{u_m^2} \right) - \frac{1}{w_j^2} \right] \\ C_{jj}^a &= -\rho g \frac{\rho}{\rho_a} \frac{g}{\omega^2} A_j w_j \tan 2w_j c \end{aligned} \quad (43)$$

where  $n$  is odd,  $j \geq 7$ ,  $s_m = \sin u_m a$  for odd  $m$ ,  $s_m = 0$  for even  $m$ ,  $S_i = 4ab$  (the area of the interface),  $A_7 = S_i$ , and  $A_j = 2ab$  for  $j > 7$ . These coefficients are symmetric. All other coefficients are trivial because of the geometric symmetry and the use of the modes in Eq. 38.

For small  $K_a$ , the leading order approximations of the coefficients, with the error of  $O(K_a^2)$ , are independent of  $\omega$  except  $C_{jj}^a$ , for  $j > 7$ , which is proportional to  $1/\omega^2$ . In particular,

$$A_{33}^a \approx \rho_a V, \quad C_{37}^a = C_{73}^a \approx \rho g S_i \quad \text{and} \quad C_{77}^a \approx -\rho g \frac{\rho}{\rho_a} \frac{g}{c_o^2} V \quad (44)$$

where  $V$  denotes the mean volume of the air in the chamber.

Often  $C_{77}^a$  is estimated by assuming an adiabatic process,  $p v^\gamma = P V^\gamma$ , where  $\gamma$  denotes the adiabatic index;  $p$  and  $v$  denote the instantaneous pressure and volume, respectively; and  $P$  denotes the static air pressure. In this case,  $C_{77}^a$  is given by:

$$C_{77}^a = \frac{-\rho g V}{\gamma(P_a/\rho g + H)} \quad (45)$$

where  $P_a$  is the atmospheric pressure and  $H$  is the submergence of the interface.